Scientific paper

Synthesis, SC XRD Based Structure Elucidation, Supramolecular Assembly Exploration Via Hirshfeld Surface Analysis, Computational and QTAIM Study of Functionalized Anilide

Muhammad Nawaz Tahir,¹ Muhammad Ashfaq,^{1*} Akbar Ali,^{2*} Chin Hung Lai,^{3,4} Bojja Rajeshwar Rao,⁵ Khurram Shahzad Munawar^{6,7} and Irshad Ali Shahid¹

¹ Department of Physics, University of Sargodha, Sargodha 40100, Pakistan

² Department of Chemistry, Government College University, Faisalabad, Pakistan

³ Department of Medical Applied Chemistry, Chung Shan Medical University, Taichung 40241, Taiwan

⁴ Department of Medical Education, Chung Shan Medical University Hospital, Taichung 402, Taiwan

⁵ Senior Chemist (Retired), Chemical Division, Kakatiya Thermal Power Project (O&M) Chelpur-506 170, Telangana State, India

⁶ Department of Chemistry, University of Mianwali, 42200, Pakistan

⁷ Department of Chemistry, University of Sargodha, 40100, Pakistan

* Corresponding author: E-mail: ashfaq.muhammad@uos.edu.pk

Received: 03-03-2023

Abstract

The anilide compound named (*Z*)-4-(2-methoxy-4-nitrophenyl)amino)-4-oxobut-2-enoic acid (**MAOA**) has been synthesized by the chemical reaction of 2-methoxy-4-nitroaniline and maleic anhydride in ethyl acetate. The synthesized compound was characterized by elemental analysis, FT-IR and UV-Vis spectroscopy, and TGA/DSC technique. Furthermore, the crystal structure was analyzed by the single crystal X-ray diffraction (SC XRD) technique. The supramolecular assembly of **MAOA** in terms of non-covalent interactions was explored by Hirshfeld surface analysis. Void analysis inferred that **MAOA** is expected to have good mechanical properties. The crystal packing environment was further investigated by interaction energy between molecular pairs and energy frameworks. Moreover, the result of the gas-phase DFT study showed that there is an intramolecular N–H···O and O–H···O hydrogen bond in **MAOA** due to the distance between D and A being smaller than the sum of their van der Waals radii. The result of the QTAIM study showed that there should also be an intramolecular CH···O hydrogen bond with a strength of 3.40 kcal/mol in **MAOA**.

Keywords: Anilide; Crystal structure; Supramolecular assembly; Non-covalent interactions; Gas-phase DFT

1. Introduction

Substituted anilines are very important chemical species that could be used as a starting material for the synthesis of valuable triazole-based medicines like fluconazole, itraconazole, voriconazole, and posaconazole. Another important method of aniline modification is the N-alkylation followed by photochemical radical cyclization reaction for the synthesis of indoles, as a precursor for the synthesis of the acetaminophen (paracetamol) that

is widely used as a medication to treat the pain and fever,³ and for the photochemical cyclization to accomplish the highly substituted indulines.⁴ Aniline could also be used as a precursor for the synthesis of quinoline which is an important heterocyclic aromatic compound with medicinal and chemical significance.⁵ Acid anhydrides are also valuable chemical building blocks with the speciality of high reactivity that can be used for the synthesis of new chemical architectures that might be used as intermediates or the

final products for utilization in the field of chemical modification specially anilides.

Anilides, mostly produced by the reaction of substituted anilines and anhydrides are well-recognized chemical building blocks in the field of medicinal chemistry because of their broad bioactive spectrum. Anilides such as MAOA having the nitro group and carboxylic acid functionality could be exciting chemical compounds as the hetero atoms might be responsible for non-covalent interactions and could also be used as potential ligands in coordination chemistry. Nitro group containing anilides have shown several biological activities like antidepressants and anticancer, analgesic and antimicrobial, caspases activators and apoptosis inducers, and anti-HIV-I agents as shown in Figure 1.

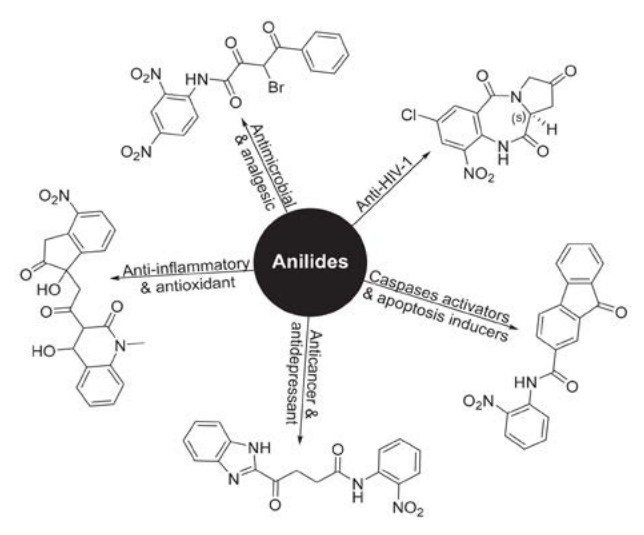


Figure 1. Anilide functionality embedded molecules with their biological potential.

Currently, the synthesis of crystalline organic compounds and their single crystal analysis together with the computational investigation are gaining enormous attention in order to predict various electronic features such as non-linear optical properties, ^{10–13} frontier molecular orbitals¹⁴ and non-covalent interactions etc. ^{15–17} Maleic anhydride could also be utilized for the N-alkylation of primary amines to produce functionalized anilides. Herein, we are presenting our findings concerning the synthesis, single crystal analysis-based structural investigation and computational exploration of the MAOA.

2. Experimental

2. 1. Materials and methods

The 2-methoxy-4-nitroaniline, maleic anhydride, and other reagents used in the current work were of analytical grade and purchased from Sigma-Aldrich, Merck, Daejung, and Alfa Aesar. The combustion analysis for the

estimation of C, H, and N was carried out using a Vario EL elemental analyzer. The melting point of the synthesized compound was measured in an open capillary using the Gallen Kamp electrochemical melting point device. Functional groups present in the sample were analyzed by using Fourier transform infrared spectroscopy from 400 to 4000 cm⁻¹ using IRSpirit-T equipped with diamond ATR (Shimadzu). The thermal data (TGA/DSC) was collected using Discovery 650 SDT simultaneous thermal analyzer (TA Instruments) with a temperature range from ambient to 400 °C. The heating rate was 10 °C/minute under a 99.999% nitrogen atmosphere with a flow rate of 50 mL/min. The absorption spectra were measured on a CE 7200 double-beam UV-Visible spectrophotometer using DMSO as a solvent. For the sake of thin-layer chromatography, the pre-coated silica was employed to monitor the progress of the chemical reaction and to ensure the purity of the product formed.

2. 2. Synthesis of (Z)-4-(2-Methoxy-4nitroanilino)-4-oxobut-2-enoic acid (MAOA)

Equimolar amounts of 2-methoxy-4-nitroaniline (1.0 mmol, 0.168 g) and maleic anhydride (1.0 mmol, 0.098 g) were dissolved separatelyin 10 mL of ethyl acetate in 50 mL of beakers. Both solutions were then mixed drop by drop with continuous stirring. After complete addition, the mixture was further stirred for 5 hours. The progress and completion of the reaction and purity of the product were continuously monitored with the help of thin-layer chromatography. The yellow solid product was then obtained by evaporation of solvent *via* a rotary evaporator. Recrystallization of the obtained product was done in methanol to get light yellow crystals (0.213 g) of good quality (Scheme 1).

MAOA: Yield: 80 %; M.P: 171 °C; Color: Light Yellow; Anal. Calc. for $C_{11}H_{10}N_2O_6$: C, 49.63; H, 3.79; N, 10.52; Found: C, 49.52; H, 3.71; N, 10.55 %; FT-IR (cm⁻¹); 3328 (νN-H), 3055 (νCH _{aromatic}), 3001 (νC-H _{alkene}), ~2970 (νC-H _{aliphatic}), 1713 (νCOO), 1615 (νC=O), 1582 (νC=C), 1552 and 1349 (νNO₂), 1017 (νC-N) [Figure S1]; UV-Vis (DMSO); λ_{max} = 360 (π - π *) [Figure S2]; TGA/DSC; 71% weight loss from 130 to 260 °C, Enthalpy (normalized); 1361 J/g, Phase change at 171 °C with heat flow -0.671 W/g, Residue 12.97% [Figure S3].

2. 3. X-ray Crystallography Details

Raw data of single crystal by X-ray was collected on Bruker Kappa Apex-II CCD diffractometer with a target made of molybdenum and $\lambda = 0.71073$ Å. APEX-II software was employed for data collection. The structure was solved and refined on SHELXT2014¹⁸ and SHELXL-2019/2,¹⁹ respectively. Refinement of all atoms other than H-atoms was performed by employing aniso-

tropic displacement parameters of atoms whereas refinement of H-atoms was performed with relative isotropic displacement parameters by using the riding model. OR-TEP-3,²⁰ PLATON²¹ and Mercury 4.0²² software were employed for the graphical representation of results.

Table 1. Crystal data and refinement parameter for **MAOA**.

| Chemical formula | $C_{11}H_{10}N_2O_6$ |
|---|----------------------|
| Molecular weight | 266.21 |
| Temperature | 296(2) K |
| Crystal system | Monoclinic |
| Space group | $P2_1/c$ |
| a (Å) | 3.8664(6) |
| b (Å) | 23.282(4) |
| c (Å) | 11.2114(17) |
| α (°) | 90 |
| β (°) | 96.461(9) |
| γ (°) | 90 |
| $V(Å^3)$ | 1132.0(3) |
| Z | 4 |
| μ (mm ⁻¹) | 0.130 |
| F(000) | 552 |
| Reflections collected | 8207 |
| Unique reflections | 2168 |
| Observed reflections $[I > 2\sigma(I)]$ | 1388 |
| Data/restraints/parameters | 2168/0/174 |
| $R_{ m int}$ | 0.078 |
| S | 1.071 |
| R_1 , wR_2 [I $\geq 2\sigma(I)$] | 0.0811, 0.1770 |
| R_1 , wR_2 (all data) | 0.1191, 0.1988 |
| | |

2. 4. Procedure of Hirshfeld Surface Analysis and Interaction Energy Between Molecular Pairs

Hirshfeld surface analysis is a unique way for the exploration of strong as well as weak intermolecular interactions in single crystals. The analysis is done on Crystal Explorer version 21.5.²³ Hirshfeld surfaces providing information about the intermolecular interactions by color coding.²⁴ We further explored the crystal packing environment by finding the interaction energy between molecules. Crystal Explorer version 21.5 is used for interaction energy calculations along with B3LYP/6-31G(d,p) electron density model. The interaction energy is the sum of four

kinds of energies named as electrostatic (E_ele), polarization (E_pol), dispersion (E_dis) and exchange repulsion (E_rep). Electrostatic energy can be attractive or repulsive whereas polarization and dispersion energy are always attractive.

2. 5. Computational Details

2. 5. 1. DFT and NBO Studies

The DFT study is utilized to examine the title compound's gas-phase structures. The DFT calculations were done using the hybrid B3LYP approach, which is a combination of the exact exchange (HF) and Becke functionals, as well as the LYP correlation functional, and is based on Becke's notion.²⁶⁻²⁸ A B3LYP calculation was performed with the basis set 6-311++G**. ²⁹ After obtaining the converged geometry, the vibrational harmonic frequencies are calculated at the same theoretical level to ensure that the imaginary frequency number is zero for the saddle point. For the study of the intrinsic electronic properties of the studied compound, the NBO analysis on the studied compound is performed at the same theoretical level. All mentioned calculations are performed by Gaussian 16.30 Moreover, the molecular conformational is acquired by Austin Model method and compared with the molecular conformation by SC XRD. The details and findings of Austin Model method are given in the supplementary information file.

2. 5. 2. QTAIM Study

The quantum theory of atoms in molecules (QTAIM) also called atoms in molecules (AIM) is a model of molecules and condensed matters. In this model, the major objects of molecules and condensed matters, i.e., atoms and bonds are naturally expressed by the distribution function of the observable electronic density of a molecule. The electron density distribution of a molecule is a probability distribution and describes the average distribution of the electronic charge in the field of attraction exerted by the nuclei. According to QTAIM, the molecular structure is revealed by the stationary points and the gradient paths of electron density. The gradient paths of a molecule's electron density are originated and terminated from the stationary points. In this study, the QTAIM analysis is performed using the multiwfn program.³¹

Scheme 1. Synthetic scheme for the (Z)-4-(2-methoxy-4-nitroanilino)-4-oxobut-2-enoic acid (MAOA).

3. Results and Discussion

3. 1. Synthesis and Analysis

A new functionalized anilide (MAOA) was synthesized by reacting 2-methoxy-4-nitroaniline with maleic anhydride in ethyl acetate under stirring conditions. The obtained yellow solid product was recrystallized in methanol to get pure crystals suitable for X-ray diffraction analysis and spectroscopic characterizations (Scheme 1).

3. 2. Single Crystal X-ray Diffraction Analysis of MAOA

The Cambridge structure database search confirmed that the crystal structure of **MAOA** is novel. The search provides a lot of crystal structures that have some similar-

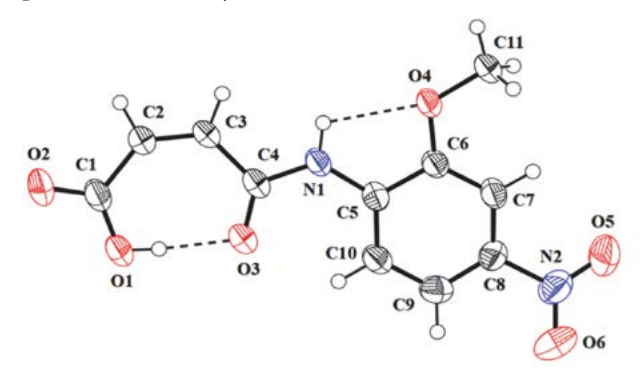


Figure 2. ORTEP diagram of **MAOA** that is drawn at the probability level of 50% with H-atoms are displayed by small circles of arbitrary radii.

ities with the crystal structure of MAOA. The crystal structure of MAOA is compared with the closely related crystal structures.

The molecular configuration of MAOA (Figure 2, Table 2) is stabilized by intramolecular N-H--O and O-H...O bonding. S(5) and S(7) H-bonded loops are formed by the intramolecular N-H--O and O-H--O bonding, respectively.³² The (Z)-4-oxobut-2-enoic acid group A (C1-C4/O1-O3) and 2-methoxyanilinic group B (C5-C11/N1/O4) are roughly planar with root mean square (r.m.s.) deviations of 0.0694 and 0.0159 Å, respectively. The corresponding dihedral angle A/B is 6.73(14)°. The nitro group C (N2/O5/O6) is twisted at the dihedral angle of 10.3(4)° with respect to group B. The substitutions on the phenyl ring make the molecule non-planar. The molecules are connected in the form of dimers through N-H-O and C-H-O bonding to form R¹₂(6) loop (Figure 3, Table 2). In both H-bonding, the acceptor O-atom is from the carbonyl O-atom (O2) of the carboxylate group (C1/O1/O2). In C-H...O bonding, the H-bond donor is from group A. The phenyl ring, carbonyl O-atoms (O3/ O4) and nitro group are not involved in any intermolecular H-bonding. Due to the intermolecular bonding, a monoperiodic infinite chain of molecules is formed with a base vector [2 0 1]. Moreover, solid-state packing is further stabilized by $\pi \cdot \cdot \cdot \pi$ stacking. The phenyl rings of the molecule present in the asymmetric unit are involved in off-set $\pi \cdots \pi$ stacking interactions with the phenyl rings of the symmetry-related molecules (1 - x, y, z and 1 + x, y, z). Inter-centroid separation of this interaction is 3.866 Å and the ring off-set range is from 1.527 to 3.866 Å as displayed

Figure 3. Packing diagram of MAOA showing dimerization of molecules.

in Figure 4. The other weak interactions such as $C-H\cdots\pi$, $N-O\cdots\pi$ and $C-O\cdots\pi$ are not found in the crystal packing of MAOA. The Cambridge structure database search provides more than 50 crystal structures that have some similarity with the crystal structure of MAOA. The close inspection of these structures inferred that 5 out of 50 have close similarity with the crystal structure of MAOA. Two structures with reference code JAYGEW33 and MNP-MAL01³⁴ have nitro-substituted phenyl rings whereas, the other two structures with reference code LAQIEU35 and SAGFIR³⁶ have disubstituted phenyl rings (nitro and chloro). The molecular configuration of JAYGEW and MNPMAL01 is stabilized by intramolecular O-H--O and C-H···O bonding along with intermolecular N-H···O and C-H···O bonding. O-H···O intramolecular H-bonding is found in LAQJEU and SAGFIR along with N-H...Cl bond-

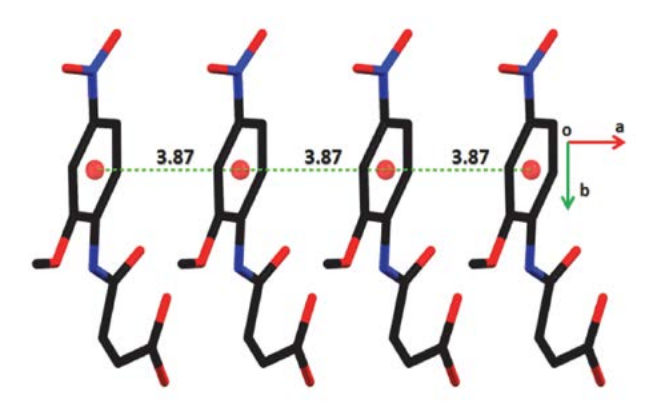


Figure 4. Graphical representation of chain along a-axis that is formed by off-set π - \cdots π stacking interactions. H-atoms are not shown for clarity. Distances are measured in Å.

ing which is present in SAGFIR. $\pi \cdots \pi$ stacking interaction is found in these four selected literature crystal structures.

Table 2. Hydrogen-bond geometry (Å, °) for MAOA.

| D—H···A | <i>D</i> —Н | HA | D···A | <(D—H···A)° |
|---------------------------|-------------|------|-----------|-------------|
| N1-H1 <i>A</i> ···O4 | 0.86 | 2.22 | 2.621 (3) | 108 |
| O1-H1···O3 | 0.82 | 1.74 | 2.545 (3) | 167 |
| N1-H1A···O ² i | 0.86 | 2.39 | 3.198 (4) | 156 |
| C3-H3···O ² i | 0.93 | 2.31 | 3.176 (4) | 154 |

Symmetry codes: (i) x - 1, $-y + \frac{1}{2}$, $z - \frac{1}{2}$.

3. 3. Hirshfeld Surface Analysis

Hirshfeld surface (HS) mapped over d_{norm} is displayed in Figure 5a. The surface uses three colors, red, white and blue to classify interatomic contacts by their strength. Red and blue spots stand for short and long contacts, respectively. The contacts for which the distance between the interacting atoms is equal to the sum of the van der Waal radii are shown by white spots on the surface. The most dominant interactions in the crystal packing are indicated by red spots on the HS whereas nearly negligible and intermediate intermolecular interactions are indicated by blue and white color, respectively. The red spot around the NH group, one of the CH of group A and the carbonyl O-atom of the carboxylate group indicate that these atoms are involved in short contacts or H-bonding. The H-bonding is represented by the green dotted line in Figure 5a. $\pi \cdots \pi$ stacking interactions can be visualized by plotting HS over the shape index. The presence of consecutive red and

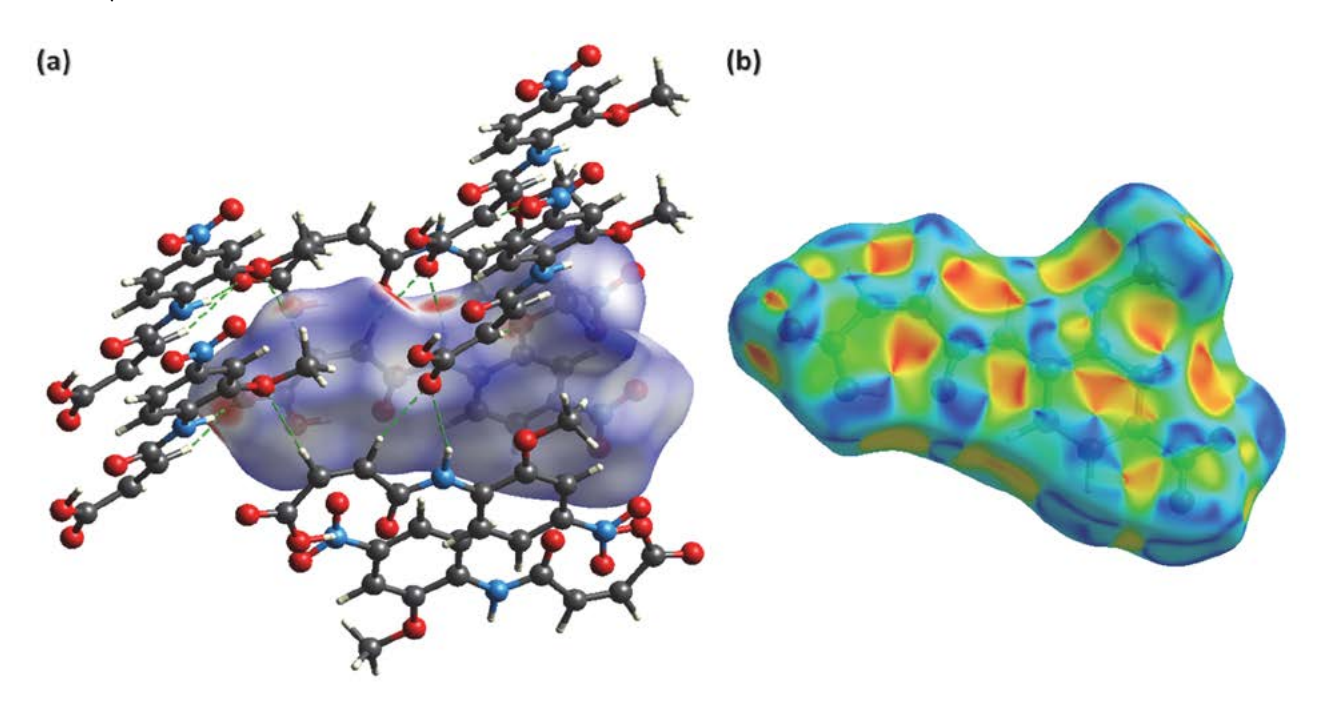


Figure 5. Hirshfeld surface plotted over (a) d_{norm} , (b) shape index.

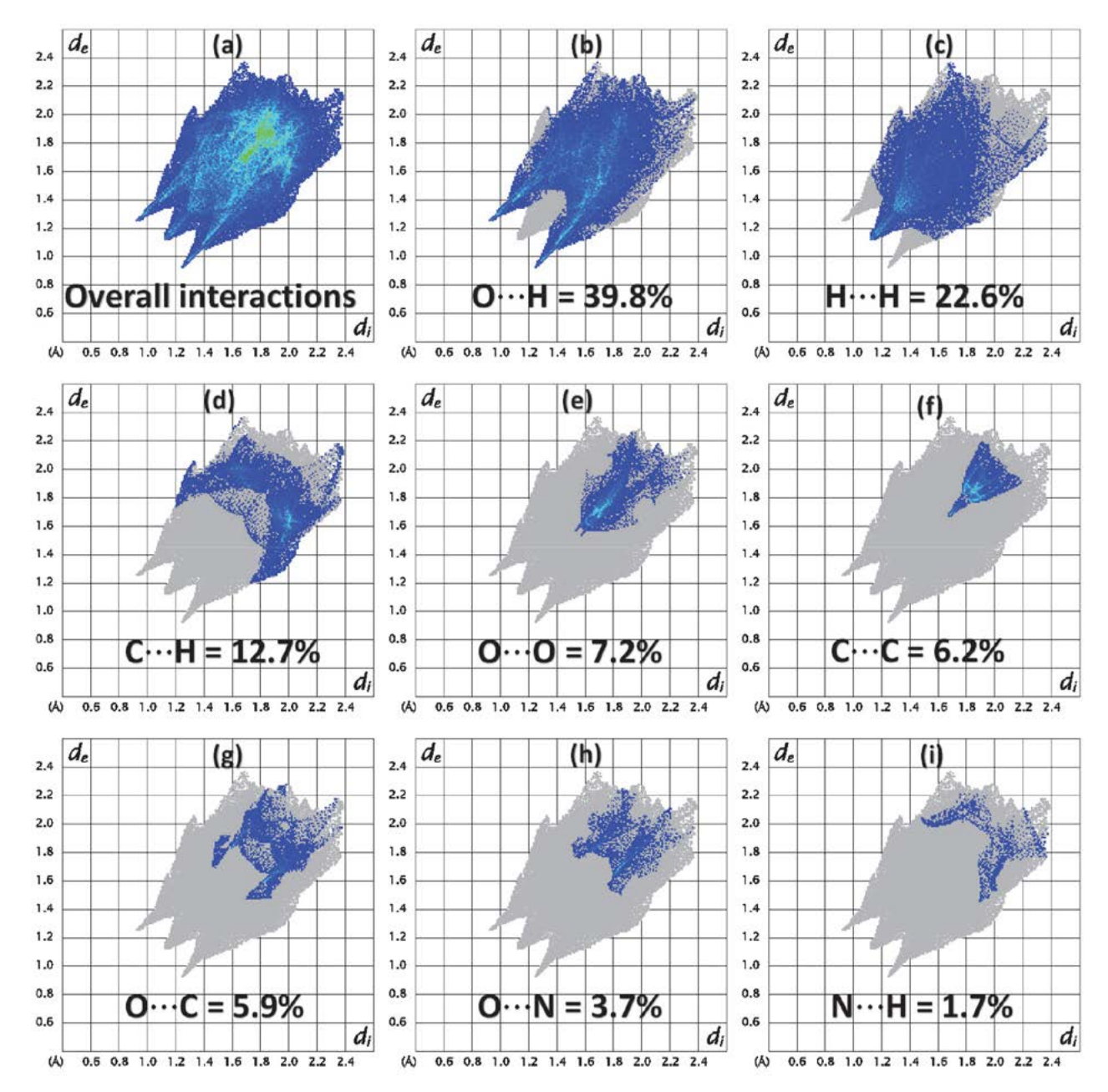


Figure 6. Two-dimensional fingerprint plots in MAOA for (a) overall interactions and (b-i) individual interatomic contacts.

blue triangular-shaped regions around phenyl rings in Figure 5b indicates that stacking interactions are present in **MAOA**.

The intermolecular interactions can be further explored with the utilization of two-dimensional fingerprint plots which is a key analysis to separately identify and quantify the interatomic contacts.^{37–40} Figure 6a is the 2D fingerprint plot for overall interactions on which short interactions contacts are shown by large spikes. In most crystal structures of organic compounds, H···H contacts are the most significant contributors in the crystal packing but in our case, the O···H contacts are the most significant contributors in the crystal packing with

a percentage contribution of 39.8% (Figure 6b). The other significant interatomic contributors responsible for the overall packing of molecules are H···H, C···H, O···O, C···C and O···C with percentage contributions of 22.6%, 12.7%, 7.2%, 6.2%, and 5.9% (Figure 6c–g), respectively. The enrichment ratio provides the tendency of the pair of chemical species in the single crystal to form crystal-packing interactions. Each pair of chemical species has a unique ability to be involved in the crystal packing. Some pairs have a higher tendency to be involved in the crystal packing interactions than others. The enrichment ratio for a pair (X, Y) is acquired by dividing the proportion of the actual contact by the proportion of the ran-

dom contact calculated theoretically.⁴¹ The results of this study are summarized in Table S1. Although the O···H contacts are the most significant contributors to the crystal packing but the contact which has the highest tendency to form crystal packing is C···C with an enrichment ratio of 2.58. The other higher tendency contacts are O···N and O···H with enrichment ratios of 2.15 and 1.26, respectively. The H···H contacts are not favorable as the enrichment ratio for this contact is less than 1.

For the sake of further exploration of the crystal packing in MAOA, the interaction of an atom of a molecule with all other atoms present in its surrounding is calculated. 42 Figure 7a gives a quantitative description of the interaction of an atom present inside the HS to the atoms present in the surrounding HS. The H-atoms present inside the HS interact strongly with atoms present in the surrounding HS with a percentage contribution of 46.6%. The quantitative contribution of other such interactions O-ALL, C-ALL and N-ALL is 33.2%, 17% and 3.2%, respectively. Figure 7b gives a quantitative description of the interaction of an atom present outside the HS with all the atoms present inside the HS. The H-atoms present outside the HS interact strongly with atoms present inside the HS with a percentage contribution of 53%. The quantitative contribution of other such interactions ALL-O, ALL-C and ALL-N is 30.6%, 14.1%, and 2.3%, respectively.

3. 4. Interaction Energy and Energy Frames Analysis

The molecule present in the asymmetric unit is taken as a reference molecule and molecules present in the vicinity of the reference molecule (3.8 Å) are taken in calculations. The results of interaction energy calculations are given in Table 3. The total energy is maximum for the molecular pairs with the center-to-center separation of 11.07 Å that are related to each other by inversion symmetry and for this pair, the hydrogen-bonded contacts are the major controller of the interaction energy as compared to the $\pi \cdot \cdot \cdot \pi$ stacking interaction. The net attractive energy is maximum for the molecular pairs with the center-to-center separation of 9.91 Å that is related to each other by symmetry $(-x, -y + \frac{1}{2}, z +$ ½). The electrostatic energy is repulsive for two molecular pairs with the center-to-center separation of 3.87 and 6.07 Å. For the molecular pair with an intermolecular distance of 3.87 Å, hydrogen-bonded contacts and $\pi \cdot \cdot \cdot \pi$ stacking interaction both are the significant controller of the interaction energy. For all other pairs, the hydrogen-bonded contacts are the significant controller of the interaction energy. The strength of a particular type of interaction energy can be visualized by energy frameworks that contained cylinders whose width is directly proportional to the strength of the interaction. 43 Figure 8 represents energy frames of the electrostatic and dispersion energy, respectively. Energy

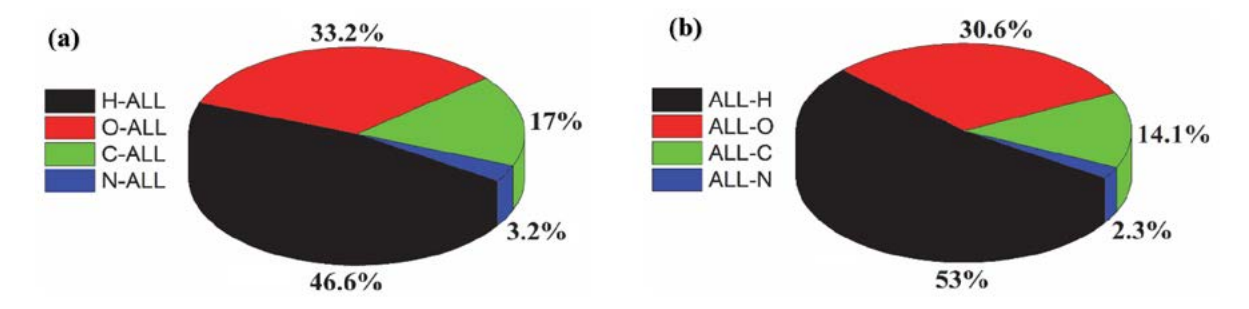


Figure 7. Graphical summary of the **(a)** Interaction of an atom present inside the HS to atoms present in the surrounding of HS, **(b)** Interaction of an atom present outside the HS to atoms present in the HS.

Table 3. Intermolecular interaction energies in kJ mol⁻¹ calculated at B3LYP/6-31G(d,p) electron density model for MAOA.

| | | | | | | | | | %E_attract contribution | | |
|-----------------------|---|-------|-------|-------|-------|-------|-------|------------|-------------------------|--------|--------|
| Colour Symmetry codes | N | R | E_ele | E_pol | E_dis | E_rep | E_tot | %E_attract | %E_ele | %E_pol | %E_dis |
| (i) | 1 | 6.07 | 1.9 | -1.6 | -23.1 | 10 | -12.8 | -24.7 | 0 | 6.48 | 93.5 |
| (ii) | 2 | 3.87 | 15.8 | -6 | -62 | 28 | -24.2 | -68 | 0 | 8.82 | 91.2 |
| (i) | 1 | 11.07 | -26.9 | -5.1 | -14.6 | 18.4 | -28.2 | -46.6 | 57.7 | 10.9 | 31.3 |
| (ii) | 2 | 11.44 | -14.8 | -2.8 | -6.7 | 5 | -19.3 | -24.3 | 60.9 | 11.5 | 27.6 |
| (iii) | 2 | 9.91 | -30.2 | -9.1 | -15.9 | 30.7 | -24.5 | -55.2 | 54.7 | 16.5 | 28.8 |
| (i) | 1 | 10.57 | -21 | -3.9 | -17.2 | 11.3 | -30.8 | -42.1 | 49.9 | 9.26 | 40.9 |
| (iii) | 2 | 9.39 | -0.8 | -5.6 | -18.4 | 13.4 | -11.4 | -24.8 | 3.23 | 22.6 | 74.2 |
| (i) | 1 | 6.80 | 13.8 | -2.5 | -17.4 | 7.9 | 4.2 | -19.9 | 0 | 12.6 | 87.4 |

Symmetry codes: (i) -x, -y, -z; (ii) x, y, z; (iii) -x, $-y + \frac{1}{2}$, $z + \frac{1}{2}$.

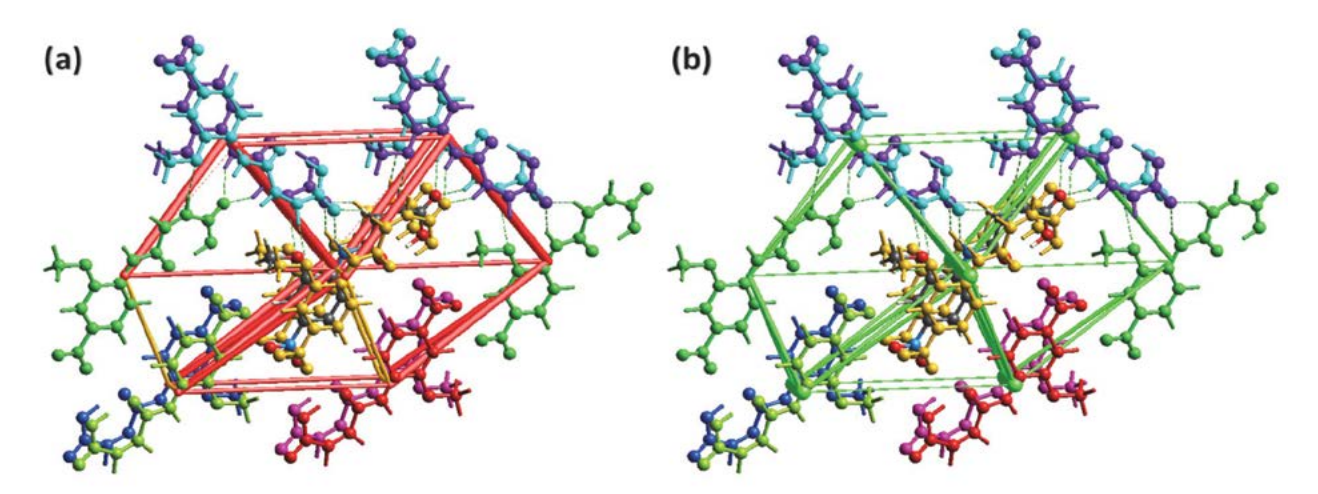


Figure 8. Energy frames for (a) electrostatic energy, (b) dispersion energy.

frames show that the contribution of the dispersion energy in defining the total interaction energy is greater than the contribution of the electrostatic energy.

3. 5. Void Analysis

The percentage of void volume in the unit cell of a compound is the demonstration of how strongly the molecules are packed with each other. Figure S4 is a graphical view of voids that is obtained by summation of electron densities of spherically symmetric atoms at the pertinent nuclear positions. 44–47 The computations of the crystal void infer that the void volume is of the order of 80.53 Å³. It is found that the calculated void volume of the entitled compound is nearly equal to 7% indicating that the crystal has a high packing factor without a large cavity in the crystal packing.

3. 6. DFT Exploration

A gas-phase DFT study was performed utilizing the B3LYP functional to rationalize the relationship between

the intrinsic electronic properties, the chemical reactivity, and the biological activities of the title compound. The B3LYP-optimized geometry of the title compound is depicted in Figure 9. Moreover, the detailed comparison between the optimized geometry and the crystallographical one could be seen in the Supporting information (Table S2). Accordingly, the B3LYP/6-311+G** theoretical level which was utilized in this study is proved to be a suitable one to investigate anilide derivatives.

According to the frontier molecular orbital theory, one can determine a molecule's nucleophilicity or electrophilicity by focusing on the highest occupied and lowest unoccupied molecular orbitals (HOMO and LUMO). As Instead of considering the total electron density as a nucleophile, evaluate the localization of the HOMO orbital since electrons from this orbital have the best probability of participating in the nucleophilic attack, whereas a site with the lowest empty orbital is a suitable electrophilic site. The title compound's frontier molecular orbital is thus studied further in this work. As depicted in Figure 10, in the studied chemical, the orbital

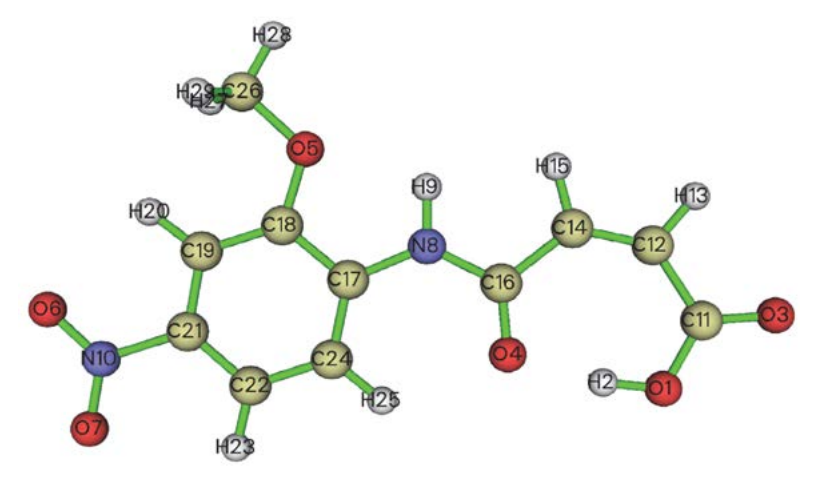


Figure 9. The B3LYP-optimized geometry of the title compound.

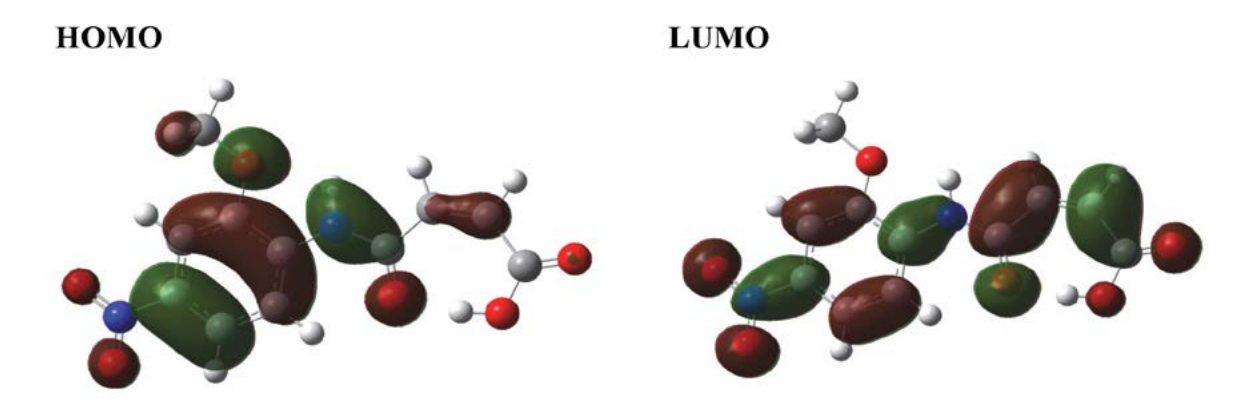


Figure 10. The HOMOs and LUMOs of the studied compound (the isovalue = 0.02 a.u.).

transfer from HOMO to LUMO belongs to a π - π * transition.

Molecular electrostatic potentials (MEPs) are essential assessments of the strength of interactions between neighboring charges, nuclei, and electrons at a specific point, allowing us to examine charge distribution and charge-related features of molecules. A graphic depiction with different colors is utilized to make the electrostatic potential data easier to understand. Electrophiles may be attracted to reading since it reflects the lowest electrostatic potential value. Blue, on the other hand, has the largest electrical potential and may be attractive to nucleophiles. The entire density of the title compound is calculated using the whole density matrix, and the resulting MEP is mapped on its surface. As depicted in Figure 11, the oxygen atoms are the most sensitive site for the attack by an electrophile among the title compound.

3. 6. 1. NBO Analysis

The second-order perturbation theory is used to analyze the relative strength of the intramolecular hydro-

gen bonds in the tested molecule in this study. When a hydrogen bond occurs, there should be an orbital interaction between the nonbonding orbital of the hydrogen-bonded acceptor (n_A) and the antibonding orbital of the H-donor bond (σ_{H-D}^*) . As a result of this orbital interaction, the H-D bond's bond strength and bond order should be reduced and decreased, respectively. Therefore, the interaction between a lone pair and the X-H antibonding orbital is summarized in Table 4. It is noteworthy that such orbital interactions with interaction energies larger than 1 kcal/ mol in the whole studied chemical are only listed in Table 4. As expected, the oxygen atom has two lone pairs (LPs) whereas the nitrogen atom has only one LP. The two LPs on the oxygen atom are represented as LP, and LP', respectively. The LPs on the oxygen atom of the methoxy group in the title chemical have three orbital interactions by interaction energies larger than 1 kcal/mol with respect to the antibonding orbitals of the C-H bond in the methyl group. However, the LPs on the oxygen atom of the methoxy group in the title chemical don't form orbital interactions by interaction energies larger than 1 kcal/mol (about 0.8 kcal/mol) with respect to the antibonding orbital of the

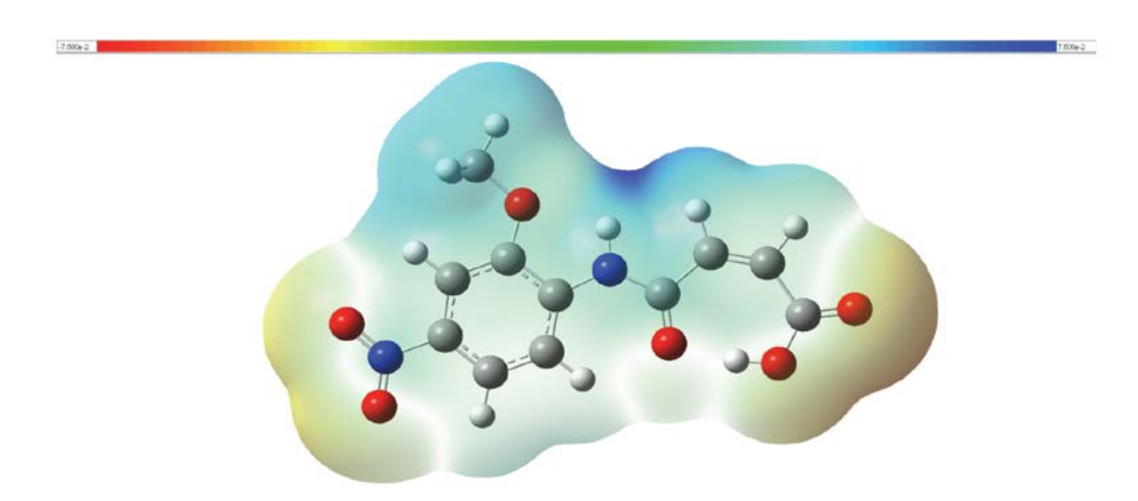


Figure 11. The MEP of the studied compound (the isovalue = 0.0004 a.u).

Table 4. The NBO results of the title compound.

| The type of n _A | The electron configuration of n _A | The orbital interaction | The interaction energy (in kcal/mol) ^b | The occupancy of $\sigma_{\text{H-D}}^*$ | The bond order of $\sigma_{\text{H-D}}^{}^{}}}$ |
|----------------------------|--|-----------------------------------|---|--|---|
| LP(O4) ^a | s(56.05%) p(43.92%) d(0.02%) | LP(O4)···σ*(O1-H2) ^a | 7.44 | 0.06057 | 0.5873 |
| LP'(O4) ^a | s(3.32%) p(96.62%) d(0.06%) | LP'(O4)···σ*(O1-H2) ^a | 25.67 | 0.06057 | 0.5873 |
| LP(O5) ^a | s(36.50%) p(63.47%) d(0.03%) | LP(O5)···σ*(C26-H27) ^a | 1.06 | 0.01534 | 0.7942 |
| LP(O5) ^a | s(36.50%) p(63.47%) d(0.03%) | LP(O5)···σ*(C26-H28) ^a | 3.23 | 0.00770 | 0.7942 |
| LP'(O5) ^a | s(0.00%) p(99.96%) d(0.04%) | LP'(O5)σ*(C26-H27) ^a | 4.11 | 0.01534 | 0.7942 |

a) Please see the atomic designations in Figure 9.

neighboring N–H bond. Moreover, the lone pair on the nitrogen atom in the title compound doesn't show orbital interactions by interaction energies larger than 1 kcal/mol with respect to any antibonding orbitals.

3. 7. QTAIM Study

The aforementioned results of the NBO analysis which show that the LPs of the oxygen atom in the methoxy group do not form orbital interactions by more than l kcal/mol with the antibonding orbital of the neighboring N-H bond motivated us to investigate whether there is no

intramolecular N-H···O hydrogen bond in the studied compound. The QTAIM study is thus performed using the Multiwfn program. Under the condition that the Poincare-Hopf relationship is satisfied, the calculated critical points (CPs) have a total of 65 (in Figure 13). There are 29, 32, 4, and 0 for the (3,–3), (3,–1), (3,+1) and (3,+3) CP, respectively. As depicted in Figure S5, the (3,–1) CP designated as points 32, 34, 61 may indicate that there is an intramolecular O1–H2···O4, C24–H25···O4, and N8–H9···O5 hydrogen bond, respectively. The QTAIM study has already been used as a powerful tool to investigate intra- or intermolecular hydrogen bonding of several sys-

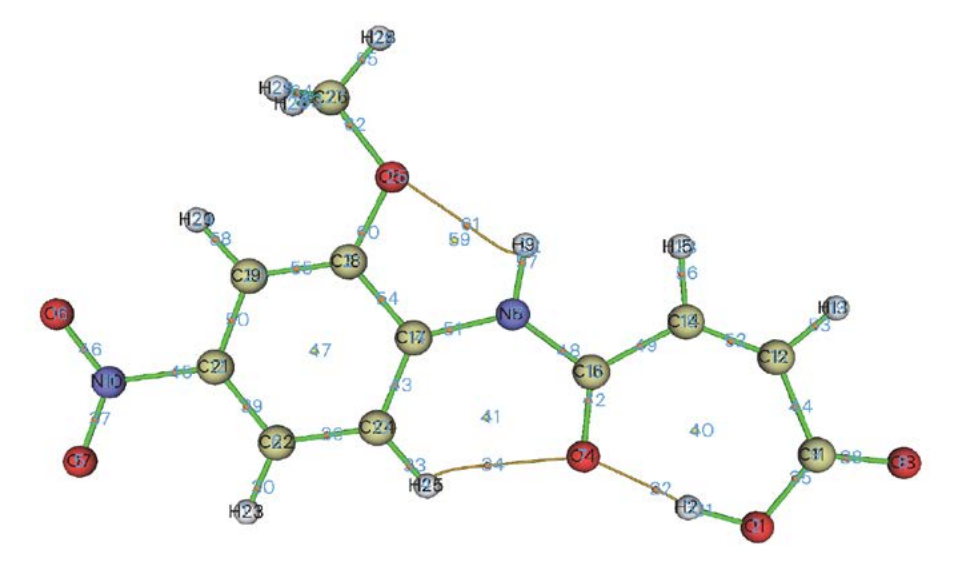


Figure 12. All the critical points of MAOA.

b) The interaction energy was calculated based on the second-order perturbation theory.

c) The listed values were the atom-atom overlap-weighted NAO bond order.

tems. $^{49-56}$ According to QTAIM, if D-H forms a hydrogen bond with A, there should be a CP between H and A. In addition, criteria about the electron density (ρ_b) and the Laplacian of electron density $(\nabla^2\rho_b)$ at BCPs have been established by Koch and Popelier to distinguish hydrogen bonding from van der Waals interactions. Moreover, Liu and coworkers have established a relationship between the hydrogen bonding strength (BE) and the electron density (ρ) at the CP corresponding to the hydrogen bond. The relationship could be described as Eq. (1) shows

BE (in kcal/mol)
$$\approx -223.08 \times \rho + 0.7423$$
 (1)

Accordingly, the strength of the aforementioned intramolecular O1–H2···O4, C24–H25···O4, and N8–H9···O5 hydrogen bonds is calculated as –11.43, –3.40, and –3.99 kcal/mol, respectively.

4. Conclusion

The (Z)-4-(2-methoxy-4-nitrophenyl)amino)-4-oxobut-2-enoic acid is synthesized and characterized by single crystal X-ray diffraction (SC XRD), UV-Vis, FT-IR, TGA/DSC techniques. SC-XRD analysis inferred that the strong intermolecular H-bonding of type O-H---O, N-H-O and comparatively weak C-H-O bonding and $\pi \cdots \pi$ stacking interactions are responsible for crystal packing. UV-Vis spectrum showed λ_{max} at 360 nm due to π - π * transitions. FT-IR result confirms the formation of the compound by showing characteristics carboxylic acid peak at 1713 cm⁻¹. TGA/DSC results represent the major weight loss (71%) in a single step from 130 to 260 °C with the loss of main fragments leaving behind residue comprised of carbon in the form of coke. It is evident from heat flow that the sample changed its phase from solid to liquid around 171 °C. Hirshfeld surface analysis shows that O-H/H-O inter-atomic contact is the most significant contributor to the overall strengthening of packing of molecules with a percentage contribution of 39.8%. The void analysis predicted that MAOA will have good mechanical properties. The interaction energy between molecular pairs and energy framework analysis showed that for the stabilization of the supramolecular assembly in MAOA, the dispersion energy is the dominant energy as compared to other types of energies. According to the results of the DFT and QTAIM studies, MAOA could be stabilized by the intramolecular O-H...O, N-H...O, and C-H... hydrogen bonds in the gas phase.

Supplementary data

CCDC 2009600 contains the supplementary crystal-lographic data for (MAOA). The data can be obtained free of charge via http://www.ccdc.cam.ac.uk/conts/retrieving. html, or from the Cambridge Crystallographic Data Cen-

tre, 12 Union Road, Cambridge CB2 1EZ, UK; fax: (+44) 1223-336-033; or e-mail: deposit@ccdc.cam.ac.uk.

Acknowledgement

Akbar Ali greatly acknowledges the support of HEC Pakistan and Khurram Shahzad Munawar is highly thankful to the University of Mianwali for characterization.

Conflict of interest: The authors declare that they have no conflict of interest.

5. References

- A. Ali, A. G. Corrêa, D. Alves, J. Zukerman-Schpector, B. Westermann, M. A. Ferreira, M. W. Paixão, *ChemComm.* 2014, 50, 11926–11929. DOI:10.1039/C4CC04678A
- G. P. da Silva, A. Ali, R. C. da Silva, H. Jiang, M. W. Paixao, ChemComm. 2015, 51, 15110–15113.
 DOI:10.1039/C5CC06329A
- 3. W. M. Lee, *J. Hepatol.* **2017**, *67*, 1324–1331. **DOI**:10.1016/j.jhep.2017.07.005
- C. A. Caiuby, A. Ali, V. T. Santana, F. W. d. S. Lucas, M. S. Santos, A. G. Corrêa, O. R. Nascimento, H. Jiang, M. W. Paixão, RSC Adv. 2018, 8, 12879–12886.

DOI:10.1039/C8RA01787E

- S. M. Prajapati, K. D. Patel, R. H. Vekariya, S. N. Panchal, H. D. Patel, RSC Adv. 2014, 4, 24463–24476.
 DOI:10.1039/C4RA01814A
- P. Theivendren, A. Subramanian, I. Murugan, S. D. Joshi, U. A. More, *Chem. Biol. Drug Des.* 2017, 89, 714–722.
 DOI:10.1111/cbdd.12894
- 7. T. Panneerselvam, S. Arumugam, M. A. Ali, K. Selvaraj, M. Indhumathy, A. Sivakumar, S. D. Joshi, *ChemistrySelect* **2017**, 2, 2341–2347. **DOI**:10.1002/slct.201601763
- 8. W. Kemnitzer, S. Cai, J. Drewe, N. Sirisoma, Substituted N-Aryl-9-Oxo-9H-Fluorene-1-Carboxamides and Analogs as Activators of Caspases and Inducers of Apoptosis, Patent Number WO2006039356A3, date of patent April 13, 2006.
- 9. H. J. Breslin, M. J. Kukla, D. W. Ludovici, R. Mohrbacher, W. Ho, M. Miranda, J. D. Rodgers, T. K. Hitchens, G. Leo, *J. Med. Chem.* **1995**, *38*, 771–793. **DOI:**10.1021/jm00005a005
- A. Ali, M. Khalid, M. F. u. Rehman, S. Haq, A. Ali, M. N. Tahir, M. Ashfaq, F. Rasool, A. A. C. Braga, ACS Omega 2020, 5, 15115–15128. DOI:10.1021/acsomega.0c00975
- B. Khan, M. Khalid, M. R. Shah, M. N. Tahir, M. U. Khan, A. Ali, S. Muhammad, *ChemistrySelect* **2019**, *4*, 9274–9284.
 DOI:10.1002/slct.201901422
- M. Khalid, A. Ali, M. Adeel, Z. U. Din, M. N. Tahir, E. Rodrigues-Filho, J. Iqbal, M. U. Khan, *J. Mol. Struct.* **2020**, *1206*, 127755. **DOI:**10.1016/j.molstruc.2020.127755
- M. Khalid, A. Ali, J. Tariq, M. N. Tahir, H. A. R. Aliabad,
 I. Hussain, M. Ashfaq, M. U. Khan, *ChemistrySelect* 2020, 5,
 10618–10631. DOI:10.1002/slct.202002653
- 14. A. Ali, Z. U. Din, M. Khalid, M. N. Tahir, E. Rodrigues-Fil-

- ho, B. Ali, S. Asim, S. Muhammad, *ChemistrySelect* **2020**, *5*, 3735–3745. **DOI**:10.1002/slct.201904757
- A. Ali, M. Khalid, S. Abid, M. N. Tahir, J. Iqbal, M. Ashfaq, F. Kanwal, C. Lu, *Crystals* **2020**, *10*, 778.
 DOI:10.3390/cryst10090778
- M. Khalid, A. Ali, S. Asim, M. N. Tahir, M. U. Khan, L. C. Curcino Vieira, A. F. de la Torre, M. Usman, *J. Phys. Chem. Solids* 2021, 148, 109679. DOI:10.1016/j.jpcs.2020.109679.
- M. Khalid, A. Ali, S. Haq, M. N. Tahir, J. Iqbal, A. A. C. Braga,
 M. Ashfaq, S. U. H. Akhtar, *J. Mol. Struct.* 2021, 1224, 129308.
 DOI:10.1016/j.molstruc.2020.129308
- 18. G. M. Sheldrick, *Acta Crystallogr., Sect. A: Found. Adv.* **2015**, *71*, 3–8. **DOI:**10.1107/S2053273314026370
- G. M. Sheldrick, Acta Crystallogr. C Struct. Chem. 2015, 71,
 3-8. DOI:10.1107/S2053229614024218
- L. J. Farrugia, J. Appl. Crystallogr. 2012, 45, 849–854.
 DOI:10.1107/S0021889812029111
- A. L. Spek, Acta Crystallogr. D Biol. Crystallogr. 2009, 65, 148– 155. DOI:10.1107/S090744490804362X
- C. F. Macrae, I. Sovago, S. J. Cottrell, P. T. Galek, P. McCabe,
 E. Pidcock, M. Platings, G. P. Shields, J. S. Stevens, M. Towler,
 J. Appl. Crystallogr. 2020, 53, 226–235.
 DOI:10.1107/S1600576719014092
- P. R. Spackman, M. J. Turner, J. J. McKinnon, S. K. Wolff, D. J. Grimwood, D. Jayatilaka, M. A. Spackman, *J. Appl. Crystallogr.* 2021, 54, 1006–1011. DOI:10.1107/S1600576721002910
- M. A. Spackman, D. Jayatilaka, CrystEngComm 2009, 11, 19–32. DOI:10.1039/B818330A
- M. J. Turner, S. Grabowsky, D. Jayatilaka, M. A. Spackman, J. Phys. Chem. Lett. 2014, 5, 4249–4255.
 DOI:10.1021/jz502271c
- A. D. Becke, *Phys. Rev. A* 1988, 38, 3098–3100.
 DOI:10.1103/PhysRevA.38.3098
- B. Miehlich, A. Savin, H. Stoll, H. Preuss, *Chem. Phys. Lett.* 1989, 157, 200–206. DOI:10.1016/0009-2614(89)87234-3
- 28. C. Lee, W. Yang, R. G. Parr, *Phys. Rev. B* **1988**, *37*, 785–789. **DOI:**10.1103/PhysRevB.37.785
- A. McLean, G. Chandler, J. Chem. Phys. 1980, 72, 5639–5648.
 DOI:10.1063/1.438980
- M. J. Frisch, G. Trucks, H. Schlegel, G. Scuseria, M. Robb, J. Cheeseman, G. Scalmani, V. Barone, G. Petersson, H. Nakatsuji, Gaussian 16, Gaussian, Inc. Wallingford, CT, 2016.
- 31. T. Lu, F. Chen, *J. Comput. Chem.* **2012**, *33*, 580–592. **DOI:**10.1002/jcc.22885
- J. Bernstein, R. E. Davis, L. Shimoni, N. L. Chang, Angew Chem. Int. Ed. Engl. 1995, 34, 1555–1573.
 DOI:10.1002/anie.199515551
- 33. J. L. Wardell, J. M. Skakle, J. N. Low, C. Glidewell, *Acta Crystallogr.*, *Sect. E: Struct. Rep. Online* **2005**, *61*, o3849–o3851. **DOI:**10.1107/S160053680503374X
- B. T. Gowda, M. Tokarčík, K. Shakuntala, J. Kožíšek, H. Fuess, *Acta Crystallogr.*, Sect. E: Struct. Rep. Online 2010, 66, o1671– o1672. DOI:10.1107/S1600536810022245
- U. Chaithanya, S. Foro, B. T. Gowda, Acta Crystallogr., Sect. E: Struct. Rep. Online 2012, 68, 0873–0873.
 DOI:10.1107/S1600536812008021

- K. Shakuntala, M. Fronc, B. T. Gowda, J. Kožíšek, *Acta Crystallogr.*, Sect. E: Struct. Rep. Online 2012, 68, 099–0100.
 DOI:10.1107/S1600536811052573
- J. J. McKinnon, D. Jayatilaka, M. A. Spackman, *ChemComm.* 2007, 3814–3816. DOI:10.1039/b704980c
- N. Kitanovski, M. Počkaj, Acta Chim. Slov. 2021, 68, 475–482.
 DOI:10.17344/acsi.2020.6634
- T. Topal, *Acta Chim. Slov.* **2021**, *68*, 88–101.
 DOI:10.17344/acsi.2020.6183
- J.-J. Wang, L.-N. Dun, B.-S. Zhang, Z.-H. Wang, H. Wang, C.-B. Li, W. Liang, *Acta Chim. Slov.* 2021, 68, 239–246.
 DOI:10.17344/acsi.2020.6438
- 41. C. Jelsch, K. Ejsmont, L. Huder, *IUCrJ* **2014**, *1*, 119–128. **DOI:**10.1107/S2052252514003327
- 42. H. Kargar, M. Fallah-Mehrjardi, R. Behjatmanesh-Ardakani, K. S. Munawar, M. Ashfaq, M. N. Tahir, *Inorg. Chim. Acta.* **2021**, *526*, 120535. **DOI:**10.1016/j.ica.2021.120535
- C. F. Mackenzie, P. R. Spackman, D. Jayatilaka, M. A. Spackman, *IUCrJ* 2017, 4, 575–587.
 DOI:10.1107/S205225251700848X
- M. J. Turner, J. J. McKinnon, D. Jayatilaka, M. A. Spackman, *CrystEngComm* 2011, 13, 1804–1813.
 DOI:10.1039/C0CE00683A
- M. Ashfaq, M. Khalid, M. N. Tahir, A. Ali, M. N. Arshad, A. M. Asiri, ACS Omega 2022, 7, 9867–9878.
 DOI:10.1021/acsomega.2c00288
- 46. H. Kargar, M. Ashfaq, M. Fallah-Mehrjardi, R. Behjat-manesh-Ardakani, K. S. Munawar, M. N. Tahir, *J. Mol. Struct.* **2022**, *1253*, 132264. **DOI**:10.1016/j.molstruc.2021.132264
- M. Ashfaq, M. N. Tahir, S. Muhammad, K. S. Munawar, A. Ali, G. Bogdanov, S. S. Alarfaji, ACS Omega 2021, 6, 31211–31225. DOI:10.1021/acsomega.1c04884
- 48. K. O. Ali, H. A. Mohamad, T. Gerber, E. Hosten, *Acta Chim. Slov.* **2022**, *69*, 905–912. **DOI:**10.17344/acsi.2022.7682
- 49. U. Koch, P. L. Popelier, *J. Phys. Chem.* **1995**, *99*, 9747–9754. **DOI:**10.1021/j100024a016
- 50. A. Saeed, M. Bolte, M. F. Erben, H. Pérez, *CrystEngComm* **2015**, *17*, 7551–7563. **DOI:**10.1039/C5CE01373A
- M. Xu, B. Zhang, Q. Wang, Y. Yuan, L. Sun, Z. Huang, J. Chil. Chem. Soc. 2018, 63, 3788–3794.
 DOI:10.4067/s0717-97072018000103788
- M. J. Javan, Comput. Theor. Chem. 2021, 1205, 113440.
 DOI:10.1016/j.comptc.2021.113440
- 53. M. K. Chaudhary, T. Karthick, B. D. Joshi, P. Prajapati, M. S. A. de Santana, A. P. Ayala, V. J. Reeda, P. Tandon, Spectrochim. Acta A Mol. Biomol. Spectrosc. 2021, 246, 118976.
 DOI:10.1016/j.saa.2020.118976
- 54. I. N. Kolesnikova, N. A. Chegodaev, P. Y. Sharanov, I. F. Shish-kov, *Chem. Phys. Lett.* **2022**, *793*, 139447. **DOI:**10.1016/j.cplett.2022.139447
- A. Jezierska, J. J. Panek, K. Błaziak, K. Raczyński, A. Koll, Molecules 2022, 27, 792–810. DOI:10.3390/molecules27030792
- 56. S. Emamian, T. Lu, H. Kruse, H. Emamian, *J. Comput. Chem.* **2019**, *40*, 2868–2881. **DOI:**10.1002/jcc.26068

Povzetek

(*Z*)-4-(2-metoksi-4-nitrofenil)amino)-4-oksobut-2-enojsko kislino (**MAOA**) smo sintetizirali z reakcijo 2-metoksi-4-nitroanilina in maleinskega anhidrida v etil acetatu. Sintetizirano spojino smo okarakterizirali z elementarno analizo, FT-IR in UV-Vis spektroskopijo in TGA/DSC analizo. Kristalno strukturo smo določili z monokristalno rentgensko difrakcijo (SC XRD). Supramolekularno strukturo **MAOA** glede na nekovalentne interakcije smo raziskali z analizo Hirshfeldove površine. Analiza praznin je pokazala, da naj bi imela **MAOA** dobre mehanske lastnosti. Okolje kristalnega pakiranja smo nadalje raziskali z interakcijsko energijo med molekularnimi pari in energijskimi mrežami. Poleg tega je rezultat DFT študije v plinski fazi pokazal, da v **MAOA** obstajata N-H···O in O-H···O intramolekularni vodikovi vezi, ker je razdalja med D in A manjša od vsote njunih van der Waalsovih radijev. Rezultat študije QTAIM je pokazal, da bi morala v **MAOA** obstajati tudi intramolekularna vodikova vez CH···O z močjo 3,40 kcal/mol.



Except when otherwise noted, articles in this journal are published under the terms and conditions of the Creative Commons Attribution 4.0 International License